Sound & Vibration 2024, 59(1), 1830.
https://doi.org/10.59400/sv1830

Article

Focusing properties of linear phase-conjugate array

Jiang Liu, Sheng Li*

State Key Laboratory of Structural Analysis, Optimization and CAE Software for Industrial Equipment, School of Naval Architecture, Dalian University of Technology, Dalian 116024, Liaoning, China
*** Corresponding author:** Sheng Li, shengli@dlut.edu.cn

CITATION

Liu J, Li S. Focusing properties of linear phase-conjugate array. Sound & Vibration. 2024; 59(1): 1830. https://doi.org/10.59400/sv1830

ARTICLE INFO

Received: 8 October 2024
Accepted: 6 November 2024
Available online: 18 November 2024

Abstract: Phase conjugation generates a backpropagating field that refocuses on the original source, rendering it an effective technique for sound source localization. In addition, linear arrays are widely used in underwater source localization. Therefore, investigating the focusing properties of a linear phase-conjugate array is crucial. This study analyzes the backpropagating field produced by phase-conjugate arrays, proposing indicators for focus bias (*FB*), focal point size (*FS*), and sidelobe interference (*SLI*) to quantitatively characterize these properties. Numerical simulations of the focusing properties of monopole phase-conjugate (PCM), dipole phase-conjugate (PCD), and perfect phase-conjugate (PCP) arrays for a single-frequency point source are conducted to evaluate the effects of array aperture, element spacing, source-to-array distance, and source bias on the different focusing properties of each array. The results indicate that focus bias and focal point size are primarily associated with the array angular aperture (determined by array aperture, source-to-array distance, and source bias); element spacing is the primary factor influencing sidelobe interference. Under identical array configurations, the focus bias of the three phase-conjugate arrays is similar, while the PCM array exhibits the smallest focal spot size, and the PCD array displays the least sidelobe interference.

Keywords: phase-conjugate array; sound source localization; focusing properties; point source; free space; waveguide

1. Introduction

Underwater source localization is a vital task in both military and civilian domains and has emerged as a key research focus in applied ocean acoustics [1]. Time reversal (TR) generates a backpropagating sound wave that refocuses on the source, establishing it as a significant method for underwater sound source localization, particularly in complex environments [2–4]. Time reversal in the time domain is equivalent to phase conjugation (PC) in the frequency domain [5]. The PC process involves digitizing the signal received by the receiving array from the sound source, time-reversing it, and retransmitting it from a transmitting array collocated with the receiving array, resulting in the backpropagated signal focusing on the original source [6]. Consequently, array configuration directly influences the focusing properties of phase-conjugate arrays, making it a crucial consideration for the practical application of phase conjugation in underwater acoustics.

Specifically, the array configuration parameters primarily include array aperture, element spacing, number of elements, array form, and so on. Each parameter affects the focusing properties of phase-conjugate arrays in distinct ways. Currently, numerous researchers have examined the influences of array configuration on the focusing properties of phase-conjugate arrays in their respective studies: Dowling et

al. [5] indicated that the conjugate array must possess sufficiently large aperture to differentiate between the various multipath directions, and the focusing quality of the conjugate array is influenced by the number and average spacing of the elements. Kuperman et al. [7] reported a focusing experiment involving a phase-conjugate array in a real ocean environment. Their study on the aperture of the time reversal mirror shows that the phase conjugation still achieves effective focusing even with a reduced aperture, although the quality of the focus degrades. Fink [2,8] described the spacing of TRM elements as a primary contributor to the quality of source localization, and the spacing should be less than λ_{min} (λ_{min} is the smallest wavelength of the sound filed) to avoid the overlapping sidelobes. Both De Rosny [9] and Fannjiang [10] investigated the focusing properties of monopole time reversal mirror (TR/M), dipole time reversal mirror (TR/D), and perfect time reversal mirror (TR/P). As the primary focus is not on array configuration, all above researches have not provided a thorough discussion on the array configuration issue. However, the array parameters mentioned here provide valuable guidance for future research on array configuration.

It is essential not only to determine the array configuration but also to clearly define the focusing properties when studying the influences of array configuration on the focusing properties of phase-conjugate arrays. Fannjiang [10] presented the full width at half maximum (FWHM) to characterize the focusing properties of the phase-conjugate sound field. FWHM is defined as the width where the sound pressure magnitude drops to half of its peak value. Harker and Anderson [11] developed a metric namely the source to field ratio (*SFR*) to quantify the quality of localization. The *SFR* measures the pressure magnitude at the original source location and compares this to the average of the magnitude of the local field surrounding the source. Similarly, Yang [12] presented the peak-to-sidelobe ratio to measure the effectiveness of temporal focusing. However, the focus of the phase-conjugate sound field exhibits bias [13] or elongation [5], making the FWHM and *SFR* not universally applicable.

Because linear array is a widely used array form in practical applications of phase conjugation [14–16], studying its focusing properties has significant importance. Based on the analysis of backpropagating fields generated by phase-conjugate arrays, the focusing properties are classified into focus bias, focal point size, and sidelobe interference. Additionally, the focus bias indicator (*FB*), focal point size indicator (*FS*), and sidelobe interference indicator (*SLI*) are proposed. Utilizing these three indicators, the focusing properties of PCM, PCD, and PCP arrays are examined in free-space and ocean waveguide environments without background noise, employing a single-frequency point source. The study primarily investigates the influences of array aperture, elements spacing, source-to-array distance, and source bias on the three focusing properties. The primary objective of this paper is to provide preliminary guidance for the configuration of linear phase-conjugate arrays. Section 2 presents the fundamental formulas and theories, along with the three indicators. In Section 3, the influences of different array parameters on the focusing properties of phase-conjugate arrays are discussed. Finally, Section 4 summarizes the main research conclusions.

2. Theory and numerical simulation

2.1. Theoretical model

This paper examines the focusing properties of phase-conjugate arrays in free-space and ocean waveguide environments without background noise, utilizing a single-frequency point source. If the ocean medium and the phase-conjugate array are motionless, more complex sources, such as a bandwidth-limited source and a moving source, can be synthesized through superposition of individual time-harmonic sources [5]. The results obtained from a single-frequency point source regarding the focusing properties of linear phase-conjugate arrays can offer preliminary guidance for the array configuration independent of specific types of sound sources.

We introduce Cartesian coordinates with horizontal coordinates x and y and depth z. Assuming a single-frequency point source is located at r_s, the sound pressure $P(r, r_s)$ at any field point $r = (x, y, z)$ in a free-space environment without background noise can be expressed using the free-space Green's function as:

$$P(r, r_s) = P_0 \frac{exp(ikR)}{4\pi R}, \tag{1}$$

where P_0 is the sound pressure magnitude, i is the unit imaginary number, $k = \omega/c$ is the wave number (ω is the angular frequency, and c is the sound velocity), and R represents the distance from the source r_s to the field point r [17].

Time reversal in the time domain is equivalent to the phase conjugation in the frequency domain, i.e.,$p(r, t)$ and $p(r, -t)$ are equivalent to $P(r, \omega)$ and $P^*(r, \omega)$. The reason that the time reversal can realize the reverse propagation and adaptive focusing of sound waves is that $p(r, t)$ and $p(r, -t)$ are both solutions of the line sound wave equation $\ddot{p} = c^2 \nabla^2 p$. According to the Helmholtz–Kirchhoff integral equation, the phase-conjugate sound field is:

$$P_{\mathrm{PC}}(r, r_s) = \int \left[G(r, r_A) \frac{\partial P^*(r_A, r_s)}{\partial n} - P^*(r_A, r_s) \frac{\partial G(r, r_A)}{\partial n} \right] dS_A, \tag{2}$$

where $r_A = (x_A, y_A, z_A)$ represents the location of array elements, S_A is microphone array area, $G(r, r_A)$ is the Green's function, $\partial/\partial n$represents the gradient operator, and * denotes conjugation.

Because the actual arrays are discrete, the phase-conjugate sound field generated by a finite discrete array including N elements is:

$$P_{\mathrm{PCP}}(r, r_s) = \sum_{n=1}^{N} [G(r, r_A^n) \frac{\partial P^*(r_A^n, r_s)}{\partial n} S_A^n - P^*(r_A^n, r_s) \frac{\partial G(r, r_A^n)}{\partial n} S_A^n], \tag{3}$$

which is called the PCP sound field. In addition, the PCD sound field is:

$$P_{\mathrm{PCD}}(r, r_s) = \sum_{n=1}^{N} [\frac{\partial P^*(r_A^n, r_s)}{\partial n} \frac{\partial G(r, r_A^n)}{\partial n} S_A^n], \tag{4}$$

and the PCM sound field is:

$$P_{\mathrm{PCM}}(r, r_s) = \sum_{n=1}^{N} [G(r, r_A^n) P^*(r_A^n, r_s)\, S_A^n], \tag{5}$$

where n is the number of array elements.

2.2. Indicators of focusing properties

In order to clearly demonstrate the specific meaning of different properties, this paper uses circular arrays and linear arrays in x–z plane to focus a point source at $r_s = (0,0,0)$ in a homogenous and free medium, following the arrangement of the TRM in Ref. [11]: the center of the circular array is the source location, and the radius of it is 12λ; the center of the linear array locates at a distance of 12λ from the source (λ is the wavelength); the sound velocity of the medium is $c = 1500$ m/s, and the density is $\rho = 1000$ kg/m^3; the frequency of the point source is $f = 100$ Hz. **Figure 1** illustrates the PCM sound fields generated by the circular array in three configurations of angular aperture (angular coverage around the source) as well as angular density (number of elements per radian), and the linear array with three configurations of aperture and element spacing. Reducing the array aperture increases the focus size (see **Figure 1a–f**). Additionally, reducing the aperture of the linear array results in a bias between focus and source (see **Figure 1d,f**). Decreasing the angular density of the circular array or the element spacing of the linear array results in significant sidelobe interference in the phase-conjugate sound field (see **Figure 1a–e**).

The results of the above simulations indicate that focus bias, focal point size, and sidelobe interference are significantly influenced by the array configuration. Currently, the metrics used to evaluate the focusing properties of a phase-conjugation array are FWHM and *SFR*. The definitions of these two metrics clearly indicate that FWHM measures the focal point size, while *SFR* quantifies the degree of interference from the sound pressure surrounding the source point, representing sidelobe interference. Additionally, the open aperture arrays generate a large and elongated focal point, as shown in **Figure 1**. The phase-conjugate fields are normalized to the sound pressure magnitude at the focus. ○ represents an element of the phase-conjugate arrays, □ represents the point source and ＋ represents the focus. The FWHM, a metric of focusing properties in a specific direction, fails to capture the overall properties of the focus. In defining the region surrounding the source for *SFR*, field points within a distance of $\lambda/4$ from the source are excluded to prevent mixing the focused pressure at the source location with the surrounding field, however, the maximum length of the focus generated by the open aperture arrays is greater than $\lambda/4$. Therefore, $\lambda/4$ is not enough to completely prevent mixing the focused pressure at the source location with the surrounding field.

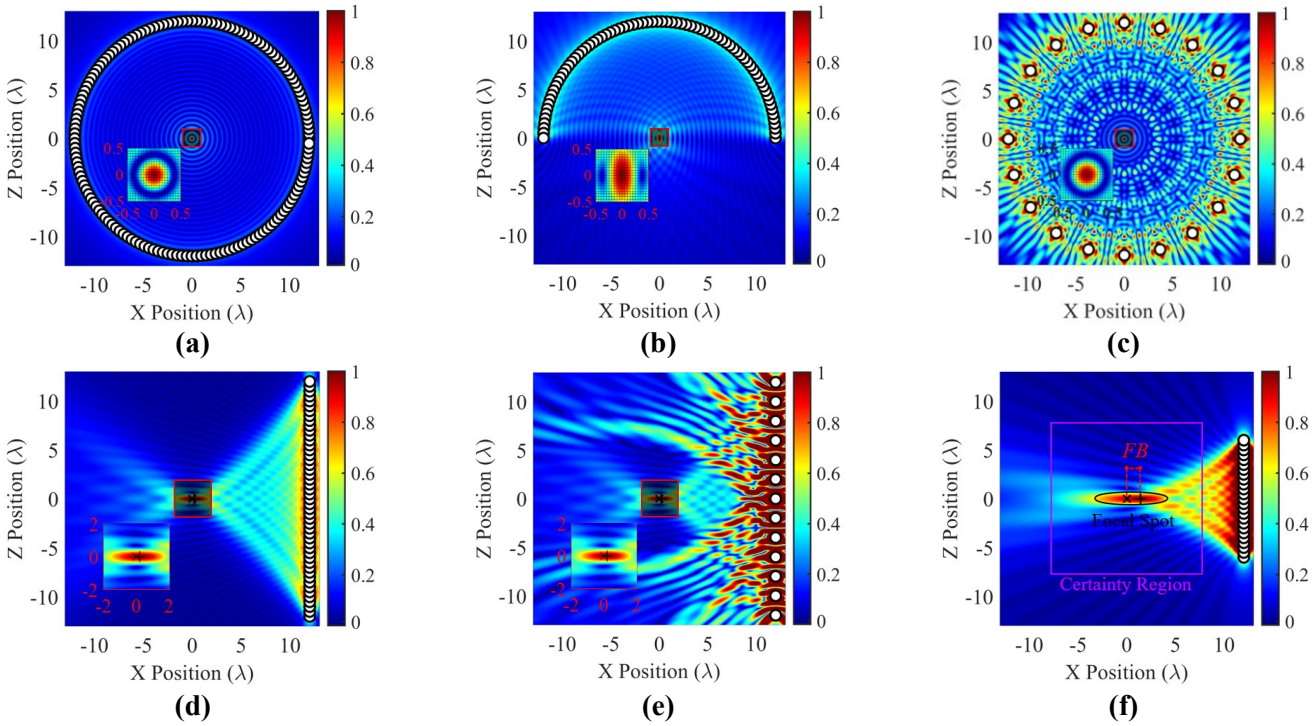

Figure 1. P CM sound pressure fields in x−z plane for three phase-conjugate circular arrays: **(a)** 2π angle aperture and 24.2 elements/radian; **(b)** π angle aperture and 24.2 elements/radian; **(c)** 2π angle aperture and 3.18 elements/radian, and three phase-conjugate linear arrays: **(d)** 24λ aperture and0.5λelements spacing; **(e)** 24λ aperture and 2λ elements spacing; **(f)** $\mathbf{12}\boldsymbol{\lambda}$ aperture and 0.5λ elements spacing.

Building on the previous analysis and the definitions of FWHM and *SFR*, this paper introduces a normalized focus area to characterize the focal point size properties of linear phase-conjugate arrays:

$$FS = \frac{S_{\mathrm{FS}}}{\lambda^2}, \tag{6}$$

where S_{FS} is the area of focus, which is defined as the region where the sound pressure magnitude is greater than or equal to 0.5 times the peak sound pressure magnitude at the focus. Essentially, this area consists of the FWHM values in all directions surrounding the source. A smaller *FS* indicates better focusing and imaging of the sound source. The region where the sound source is likely to be located is referred to as the certainty region, while the difference between the certainty region and the focus is termed the surrounding region.

We propose the ratio of the average sound pressure magnitude in the surrounding region to the peak sound pressure magnitude at the focus to characterize the sidelobe interference feature.

$$SLI = \frac{\frac{1}{M}\sum_m |P(r_m)|}{|P_F|}, \tag{7}$$

where M is the number of field points in the certainty region, r_m represents the mth filed point's location, P_F is the sound pressure magnitude at the focus. $SLI = 1$ implies that the magnitude of the focus equals the average magnitude of the nearby field, making the focus indistinguishable from the surrounding field.

In addition, the normalized distance between the focus and the source is introduced to characterize the focus bias feature:

$$FB = \frac{|r_F, r_S|}{\lambda}, \tag{8}$$

where $r_F = (x_F, 0, z_F)$ is the focus location. A smaller *FB* indicates a smaller focus bias. In this paper, half a wavelength is seen as the threshold. When $FB \leq 0.5$, the focusing of the source is considered to have sufficient accuracy. The definitions of the focus, certainty region, and the distance between the focus and source are illustrated in **Figure 1f**. It is important to emphasize that focal point size and sidelobe interference should only be discussed when the focus bias satisfies the accuracy requirements. In other words, *FB* indicates the existence of focusing, while *FS* and *SLI* indicate the quality of focusing.

3. Results and discussion

The focusing quality of a phase-conjugate array depends on parameters such as the number of array elements [5], element spacing [3,5,8], array aperture (defined as array length in linear arrays and angle relative to the source in circular arrays) [3,11], source azimuth angle [3], and the angular density of the elements relative to the source [11]. In a discrete linear array with uniform element spacing, the number of elements, element spacing, and array aperture are interdependent, meaning any one can be determined if the other two are known. The source azimuth angle can be defined by the distance between the source and the array, along with the offset distance of the source from the array center. Thus, this paper defines array aperture L, element spacing d, the source-to-array distance d_{AS}, and source bias b to describe the configuration of a linear phase-conjugation array (see **Figure 2**).

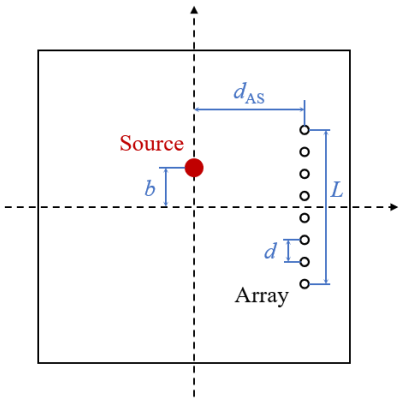

Figure 2. Definition schematic diagram of four linear array parameters: Array aperture L, elements spacing d, source-to-array distance d_{AS} and source bias b.

This section studies the influences of L, d, d_{AS}, and b on focusing property indicators *FB*, *FS*, and *SLI* through numerical simulation of the phase-conjugate sound fields generated by PCM, PCD, and PCP arrays. The default parameter settings for the numerical simulations in this section are presented in **Table 1**, where $\lambda = c/f = 15$ m. In investigating the influences of array parameters on focusing

properties, only the parameter of interest is varied, while all other values remain consistent with the defaults listed in **Table 1**.

Table 1. Default values of source, medium and array parameters in numerical simulation.

Source	Type	Sound pressure Magnitude P_0	Frequency f	Location (x, y, z)
	Point Source	1 Pa	100 Hz	(0, 0, 0)
Medium	Type	Sound Velocity c	Density ρ	Certainty Region
	Uniform and Free	1500 m/s	1 kg/m^3	24 λ × 24 λ
Array	Aperture L	Elements spacing d	Source-to-array distance d_{AS}	Source bias b
	56 λ	1/2 λ	13 λ	0 λ

3.1. Influence of array parameters on focus bias

Among the three focusing properties defined in this paper, focus bias indicates whether the sound field generated by a phase-conjugate array is directed toward the source. Consequently, this paper first examines the influence of array parameters on focus bias. The parameterized scan values for L, d, d_{AS}, and b are presented in **Table 2**. The complex sound pressure and its gradient at each element of the three phase-conjugate arrays are first calculated by substituting the source and array locations into Equation (1). Next, the sound pressure amplitudes of the PCP, PCD, and PCM sound fields throughout the certainty region are determined using Equations (3), (4), and (5). Finally, the *FB* values for the phase-conjugate arrays under varying array parameters are calculated using Equation (8).

Table 2. Values of parameters in numerical simulation for the influence of array parameters on focus bias.

Array Parameter	Values setting	Other parameters setting
L (λ)	Range = [0:60], Resolution = 1	-
d (λ)	{1/8, 1/4, 1/2} & Range = [1:56], Resolution = 0.5	Certainty region is a 4λ × 4λ square[1]
d_{AS} (λ)	Range = [13:60], Resolution = 1	-
b (λ)	Range = [0:60], Resolution = 1	-

The variations of *FB* with respect to different array parameters for the three phase-conjugate arrays are illustrated in **Figures 3–6**. **Figure 3** illustrates the influence of array aperture on focus bias. In **Figure 3a**, when $L < 16\lambda$, the *FB* values of both PCM and PCP arrays exceed 12 and surpass than 0.5 (the accuracy focusing tolerance). When $L < 17\lambda$, the *FB* value of the PCP array is significantly greater than the accuracy focusing tolerance. As L increases to 16λ, the *FB* values of both PCM and PCP array drop sharply and gradually approach 0, while this phenomenon for the PCP array occurs at $L \geq 17\lambda$. **Figure 3b** further demonstrates that when $FB \leq 0.5$, the *FB* values of all three phase-conjugate arrays decrease stepwise as L increases. **Figure 4** illustrates the influence of source bias on focus bias. *FB* increases as b increases (see **Figure 4b**), when b exceeds a certain value (29λ for PCM array, 24λ for PCD array, and 26λ for PCP array), the focus bias

suddenly increases, resulting in the failure of the three phase-conjugate sound fields to focus (see **Figure 4a**). **Figure 5** illustrates the influence source-to-array distance d_{AS} on focus bias indicator *FB*. As shown in **Figure 5**, *FB* increases stepwise as d_{AS} increases, and the focus bias remains nearly consistent across the three phase-conjugate arrays. The influence of element spacing on focus bias is shown in **Figure 6**. *FB* remains unchanged as the element spacing increases (see **Figure 6b**). When the element spacing exceeds a certain value (11λ for PCM and PCP arrays, 9.5λ for PCD arrays), *FB* suddenly increases, causing the three phase-conjugate sound fields to lose their focus (see **Figure 6a**). Together with **Figure 1d,e**, it is evident that the influence of element spacing on focus bias is attributable to sidelobe interference. When the element spacing is sufficiently large to generate grating lobes (side lobes with sound pressure amplitudes equal to that of the main lobe), the focus will shift significantly. Conversely, when the element spacing is small enough to avoid generating grating lobes, the element spacing has no influence on focus bias.

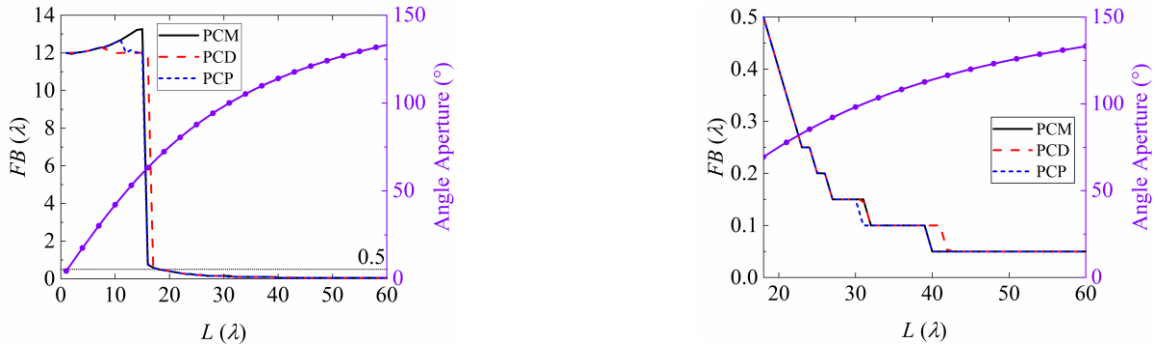

Figure 3. Influence of aperture *L* and angle aperture on focus bias indicator *FB* for **(a)** all apertures from 0 to 60λ; **(b)** apertures where *FB* is less or equal than 0.5.

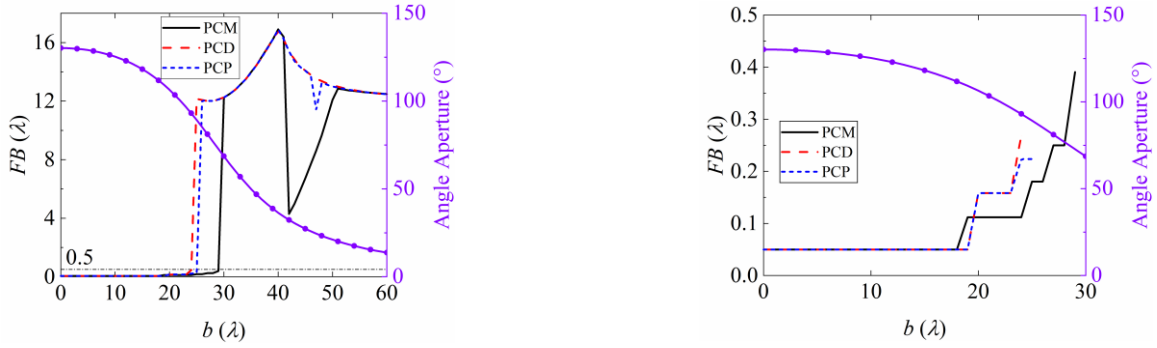

Figure 4. Influence of source bias *b* and angle aperture on focus bias indicator *FB* for **(a)** all biases from 0 to 60λ; **(b)** biases where *FB* is less or equal than 0.5.

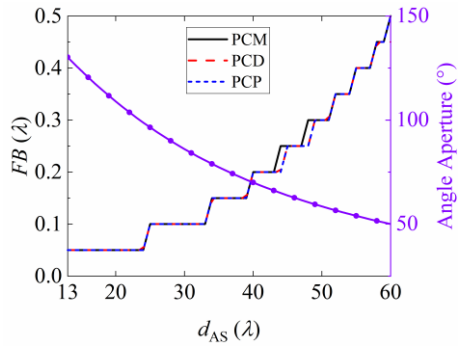

Figure 5. Influence of source-to-array distance d_{AS} and angle aperture on focus bias indicator *FB* for all distances from 13λ to 60λ.

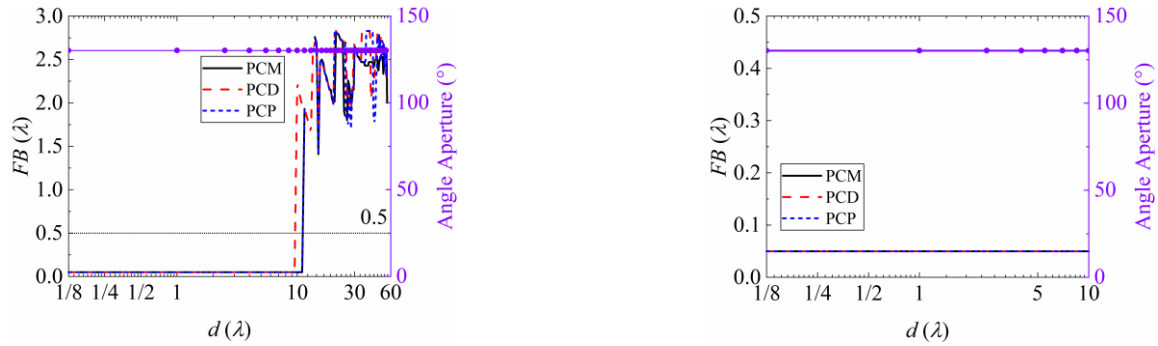

Figure 6. Influence of elements spacing *d* and angle aperture on focus bias indicator *FB* for **(a)** all spacings from 1/8λ to 60λ; **(b)** spacings where *FB* is less or equal than 0.5.

By introducing the concept of angular aperture from circular arrays to linear arrays, we define the angle of the linear array relative to the source as its angular aperture. The variations of the angular aperture with L, b, d_{AS}, and d are illustrated in **Figures 3–6**. By comparing the changes in *FB* and angular aperture, we observe that the focus bias decreases as the angular aperture increases, and vice versa, provided that the focus bias is below the focusing tolerance, i.e., $FB \leq 0.5$. The effects of L, b, d_{AS}, and d on *FB* are attributed to changes in the angular aperture of the linear array. Specifically, L is directly proportional to the angular aperture, b and $d_{AS}$are inversely proportional to the angular aperture, and d has no effect on the angular aperture when L is fixed.

In summary, the influences of array aperture, element spacing, source-to-array distance, and source bias can be uniquely represented by the angular aperture of the linear array and its effect on the focus bias property of a linear phase-conjugate array. To achieve accurate focusing on a single-frequency point source with a linear phase-conjugate array, a sufficiently large angular aperture must be ensured.

3.2. Influence of array parameters on focal point size

When the focus bias meets the accuracy requirements, the focusing quality of a phase-conjugate array is determined by the focal point size and sidelobe interference. This subsection employs the parameter settings from **Table 2** and the method outlined in Section 3.1 to numerically obtain the focal point size indicator (*FS*) for PCM, PCD, and PCP arrays. As a quality indicator of source focusing, *FS* is

meaningful only when the sound field generated by a phase-conjugate array can accurately focus on the source, i.e., when $FB \leq 0.5$. Therefore, the range of array parameters in **Table 2** is restricted to the values where $FB \leq 0.5$:$L \in [18:60]\lambda$, $d_{\mathrm{AS}} \in [13:60]\lambda$, $d \in \{1/8,1/4,1/2,[1:10]\}\lambda$, and $b \in [0:30]\lambda$.

Figure 7 illustrates the *FS* values and linear array angular apertures under different array parameters$L$, d, d_{AS}, and b. *FS* is negatively correlated with L, while positively correlated with angular aperture (see **Figure 7a**). *FS* is positively correlated with d_{AS}, whereas the angular aperture is negatively correlated with d_{AS} (see **Figure 7c**). *FS* is positively correlated with b, while the angular aperture is negatively correlated with b (see **Figure 7d**). When the array aperture is fixed, d has a minimal influence on *FS* and angular aperture (see **Figure 7b**). Considering the relationship between the angular aperture and *FS* shown in **Figure 7**, it is evident that *FS* is negatively correlated with the angular aperture. The focal point size of the sound field produced by a phase-conjugate array decreases as the angular aperture increases. Moreover, under the same array parameter settings, the phase-conjugate sound field generated by the PCM array exhibits the smallest focal point size, while the PCD array exhibits the largest. **Figure 8** shows the normalized sound pressure magnitude of the phase-conjugate sound field generated by the PCD array in the x–z plane when d is 8λ, 8.5λ, 9λ, or 9.5λ. The significant increase in *FS* for the PCD array in **Figure 7 b** can be explained by **Figure 8**. The increase in element spacing results in side lobes near the original focus that have magnitudes greater than or equal to 0.5 times the peak focus pressure, leading to distortion of the focus and a significant increase in focal point size.

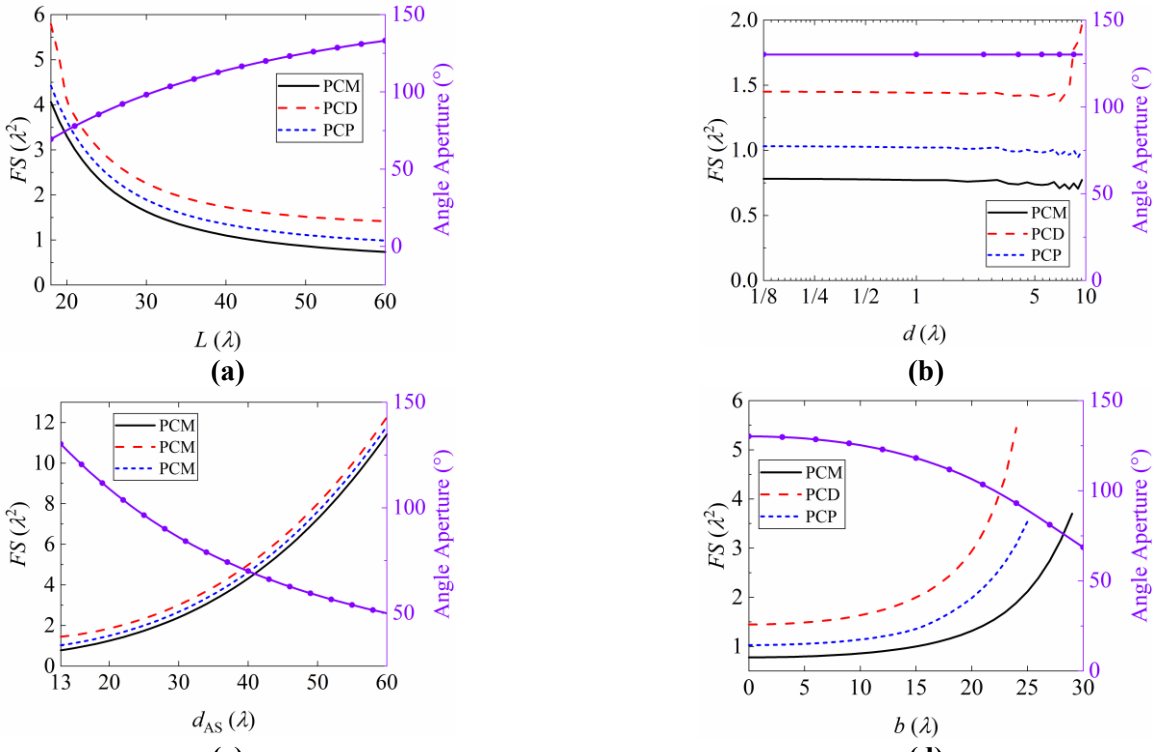

Figure 7. Influence of **(a)** aperture L; **(b)** elements spacing d; **(c)** source-to-array distance d_{AS}; **(d)** source bias b on focal point size indicator *FS* for array parameter values where *FB* is less or equal than 0.5.

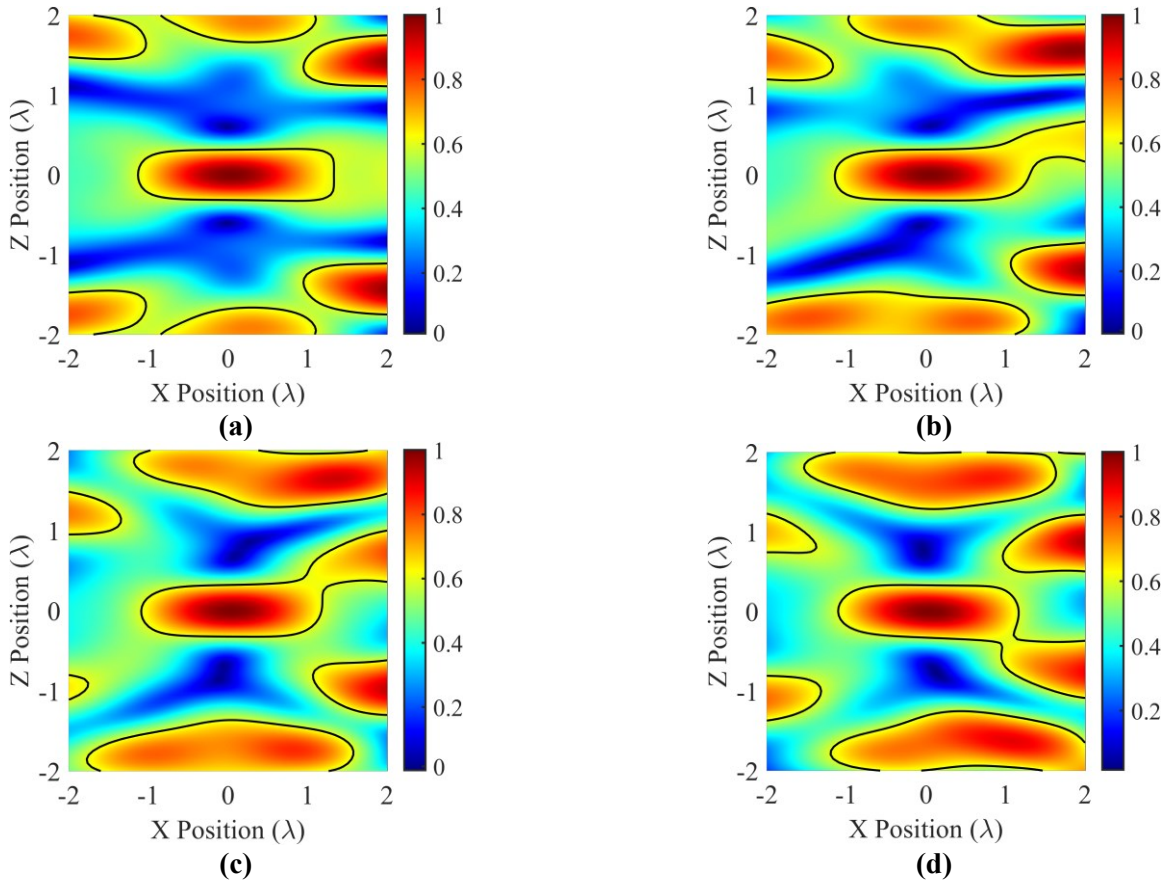

Figure 8. PCD sound pressure magnitude fields in x–z plane when element spacing d is **(a)** 8λ; **(b)** 8.5λ; **(c)** 9λ; **(d)** 9.5λ. These phase-conjugate fields are normalized to the sound pressure magnitude at the focus.

In summary, the PCM array exhibits the smallest focal point size among the three arrays analyzed. The influences of array aperture, element spacing, source-to-array distance, and source bias can be uniquely characterized by the influence of the angular aperture of the linear array on focal point size of a linear phase-conjugate array, and the focal point size is negatively correlated with the angular aperture.

3.3. Influence of array parameters on sidelobe interference

This subsection utilizes the parameter settings from **Table 2** and the methodology described in Section 3.1 to numerically compute the sidelobe interference indicator (*SLI*) for PCM, PCD, and PCP arrays. **Figure 9** illustrates the *SLI* values and angular apertures of the linear array under various array parameters L, d, d_{AS}, and b, with the parameters values specified when $FB \leq 0.5$. The sidelobe interference properties of acoustic fields generated by the three phase-conjugate arrays are minimally influenced by array aperture, source-to-array distance, and source bias (see the results shown in **Figure 9a**,**c**,**d**). The influence of element spacing on sidelobe interference exhibits a critical threshold: when the element spacing is below this threshold, *SLI* reaches its minimum and remains unaffected by further changes in element spacing; when the element spacing exceeds this value, *SLI* becomes positively correlated with element spacing (see **Figure 9b**). Additionally, except when the element spacing is greater than 6λ, the PCD array generates the least sidelobe interference, while the PCM array exhibits the most

under identical array parameter settings. However, when the element spacing exceeds 6λ, the PCM array generates the least sidelobe interference, while the PCD array exhibits the most.

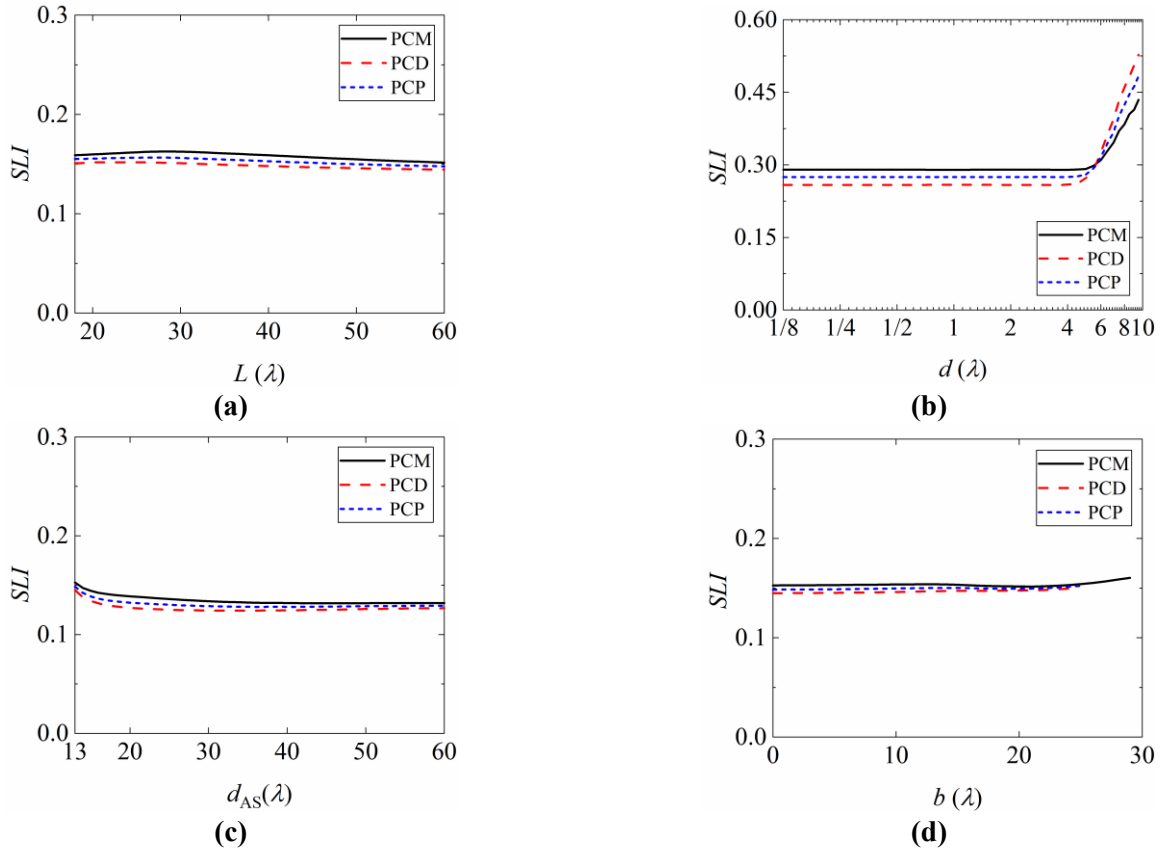

Figure 9. Influence of **(a)** aperture L; **(b)** elements spacing d; **(c)** source-to-array distance d_{AS}; **(d)** source bias b on sidelobe interference indicator *SLI* for array parameter values where *FB* is less or equal than 0.5.

The preceding study examines the influences of various array parameters on sidelobe interference within a consistent certainty region of $4\lambda \times 4\lambda$. However, the size of the certainty region affects the required number of elements in a linear phase-conjugate array to achieve optimal focusing quality [11]. Since the array aperture and element spacing uniquely determine the number of elements, and given that the array aperture has a relatively minor influence on sidelobe interference (see **Figure 9a**), the following discussion focus exclusively on how the area of the certainty region influences element spacing. The *SLI* values for the focusing acoustic fields generated by three phase-conjugate arrays with varying element spacings are numerically obtained in certainty regions of six different sizes, as shown in **Figure 10**. The element spacing values in **Figure 10** correspond to the condition when $FB \leq 0.5$. As shown in **Figure 10**, the element spacing required to achieve the minimum *SLI* increases as the size of certainty region decreases for all three phase-conjugate arrays. Similarly, the required element spacing also increases to accurately focus on the source when $FB \leq 0.5$. In other words, improved prior knowledge of the source implies larger element spacing or fewer elements for a fixed array aperture.

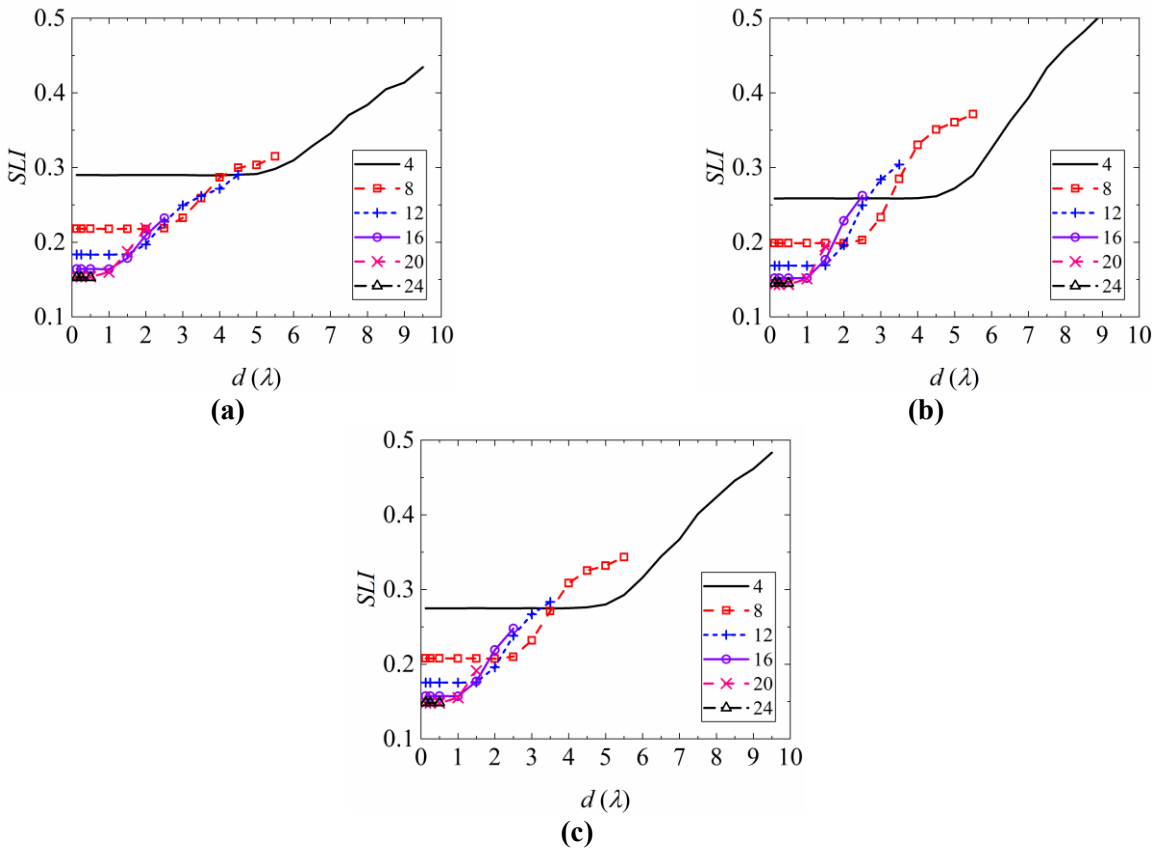

Figure 10. Sidelobe interference indicator *SLI* values for elements spacings where *FB* is less or equal than 0.5 of **(a)** PCM; **(b)** PCD; **(c)** PCP in six certainty regions.

4. Simulation in underwater environment

The simple simulations described above are highly idealized. The real ocean is a much more complicated acoustic environment than a free-space environment. To illustrate the practicality of the proposed metrics, we employ *FB*, *FS*, and *SLI* to simulate the focusing properties of a point source within a waveguide. The waveguide is a 216 m deep water layer between a free surface and the ocean bottom, which is modeled as a 23.5 m thick sediment layer, overlaying an 800 m thick mudstone layer [18]. **Figure 11** illustrates the sound speed profile of the water layer and the geo-acoustic parameters (density, attenuation, and sound speed *c*) of the ocean bottom, which are chosen to approximate the range-independent SWellEx-96 Event S5 data set [18–20]. In the waveguide model, a simulation scenario is set up as shown in **Figure 12**. A harmonic point source with a frequency of 100 Hz is placed at (8 km, 100 m), and the generated sound field is recorded by a vertical line array (VLA) located at 0 km. The physical aperture of the array is denoted as *L*, and the element spacing is denoted as *d*. The complex sound pressure at the VLA and the Green's functions between the source and array elements are computed using the Range-independent Acoustic Model (RAM) parabolic equation code. The computational domain's horizontal range and depth resolution are set to 50 m and 1 m, respectively.

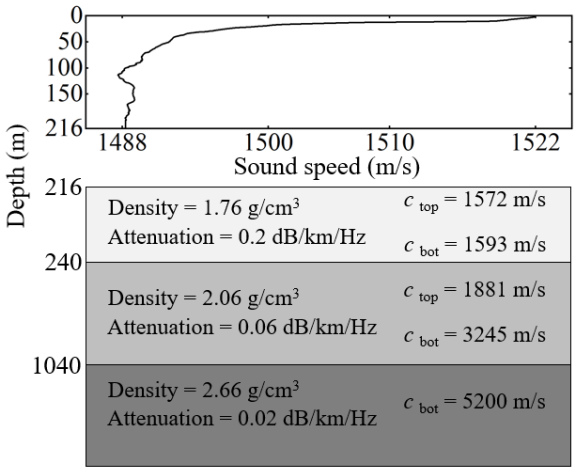

Figure 11. Waveguide with sound speed profile and geo-acoustic parameters for range-independent SWellEX-96 Event S5.

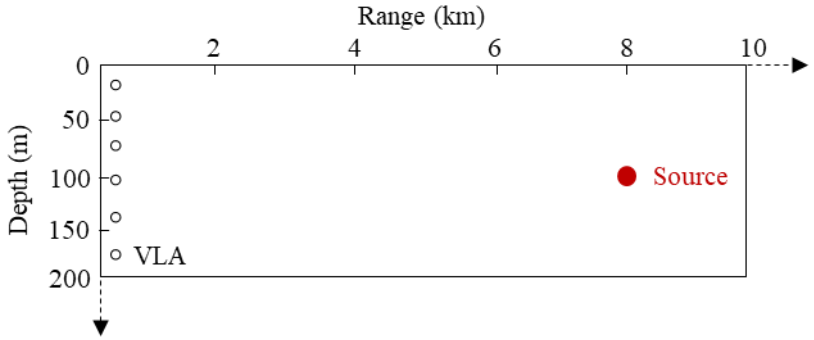

Figure 12. Schematic diagram of the source and vertical line array (VLA) arrangement in the ocean waveguide model.

To analyze the impact of different array parameters on the focusing properties, three different VLA configurations are set: Configuration 1, L = 180 m, d = 5 m (less than half the wavelength $\lambda/2$ at 100 Hz for a sound speed of 1488 m/s in water); Configuration 2, L = 180 m, d = 20 m (greater than the wavelength λ); Configuration 3, L = 100 m, d = 5 m. Phase conjugation is performed on the complex sound pressure measured by the three VLA configurations and the Green's functions of the ocean acoustic environment using Equation (5). This yields a PCM phase-conjugated sound field that propagates backward and focuses at the source location. The focal point size (*FS*), sidelobe interference (*SLI*), and focus bias (*FB*) indicators of the certainty region of phase-conjugated sound field are then calculated using Equations (6)–(8).

Figure 13 illustrates the phase-conjugated sound fields generated by the three VLA configurations, along with the focusing property indicators. From the figure, it is evident that all three arrays achieve a focusing effect at the source location, indicated by the black box, with minimal focus bias. For Configurations 1 and 2, which have the same aperture but different element spacing, Configuration 2 exhibits a higher *SLI* compared to Configuration 1, indicating stronger sidelobe interference. However, both configurations have similar *FS*, consistent with the conclusion that element spacing primarily affects sidelobe interference. For Configurations 1 and 3,

which have the same element spacing but different aperture, Configuration 3 shows larger sidelobe interference and focal point size compared to Configuration 1. This result deviates from the conclusion that aperture mainly affects focal point size in a free-space environment. The reason for this difference is that, in an ocean waveguide environment, the sound waves have multiple propagation paths to a given point, effectively increasing the aperture of the array compared to a free space. This alters the actual element spacing in the computation, thus influencing the sidelobe interference properties. This also further explains the relatively small differences in focal point size among the three arrays.

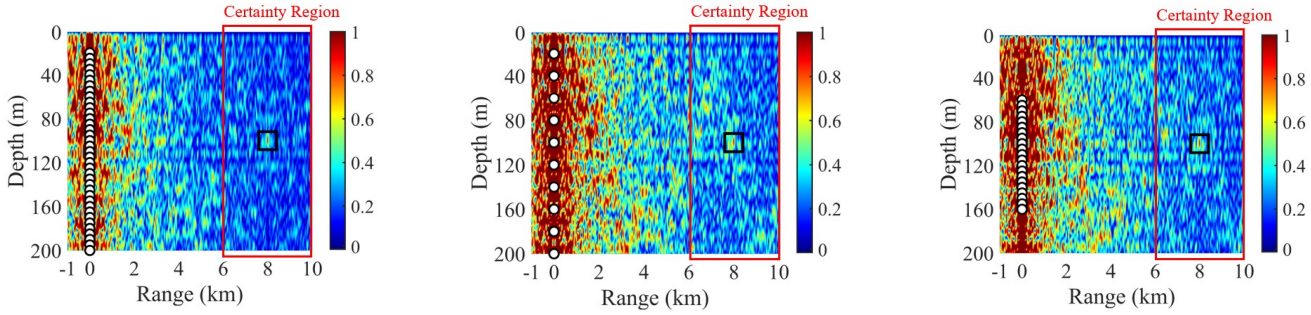

FB = 0.07 *FS* = 2.22 *SLI* = 0.21 **(a)** Configuration 1

FB = 0.07 *FS* = 2.24 *SLI* = 0.27 **(b)** Configuration 2

FB = 0.07 *FS* = 2.74 *SLI* = 0.26 **(c)** Configuration 3

Figure 13. PCM sound fields generated by VLAs with **(a)** Configuration 1; **(b)** Configuration2; **(c)** Configuration 3 and their focusing property indicators *FB*, *FS*, and *SLI* among certainty region.

The phase-conjugate sound fields are normalized to the sound pressure magnitude at the focus. ○ represents an element of the phase-conjugate arrays, and □ represents the source location.

5. Conclusion

This paper introduces three focusing indicators (*FB*, *FS*, and *SLI*) to quantitatively assess the focus bias, focal point size, and sidelobe interference of phase-conjugated sound fields generated by linear arrays in both ideal free-space and ocean waveguide models. Additionally, the influences of different array parameters on focusing properties are investigated using these indicators. Key findings include:

(1) Focus bias and focal point size are primarily related to the array angular aperture (determined by array aperture, source-to-array distance, and source bias), both decreasing as the angular aperture increases;

(2) Sidelobe interference is mainly influenced by element spacing, exhibiting an optimal value beyond which further reductions yield minimal improvements, and the optimal element spacing increases as the certainty region area decreases, indicating that better prior knowledge of the source permits fewer elements;

(3) Among PCM, PCD, and PCP arrays, the PCM array has the smallest focal point size, while the PCD array shows the least sidelobe interference at optimal element spacing.

These insights offer guidance for optimizing arrangement of linear arrays in phase-conjugate source localization technology. However, the influence of array parameters on focusing properties varies by environment. For example, in an ocean

waveguide environment, the multipath propagation effect diminished the impact of array aperture on focal point size compared to an ideal free-field environment. Therefore, targeted optimization of linear array parameters should be performed for various environments, using the focusing indicators as minimization objectives in the design process. Future research will focus on developing adaptive or dynamic array configurations that respond to real-time environmental changes, thereby enhancing the practical application of these theoretical indicators.

Author contributions: Conceptualization, JL and SL; methodology, JL and SL; software, JL and SL; validation, JL; formal analysis, JL; investigation, JL; resources, SL; data curation, JL; writing—original draft preparation, JL; writing—review and editing, JL; visualization, JL; supervision, SL; project administration, SL; funding acquisition, SL. All authors have read and agreed to the published version of the manuscript.

Conflict of interest: The authors declare no conflict of interest.

Note

[1] The elements spacing required to achieve focusing without side-lobe interference increases as the certainty region decreases (Section 3.3). Therefore, when studying the influence of elements spacing on focusing properties, a $4\lambda \times 4\lambda$ square certainty region is used. This ensures that there are sufficient numerical data available to discuss the influence of elements spacing within the elements spacing values setting in **Table 2**.

Nomenclature

λ	Wavelength	n	Number of elements
P	Sound pressure in frequency domain	m	Number of points in certainty region
G	Green's function	n	Unit normal vector
S	Area	r	Position of a field point
N	Total number of array elements	x, y, z	Cartesian coordinates
R	Distance of field points	p	Sound pressure in time domain
M	Total number of points in certainty region	k	Wave number
FB	Focus bias indicator	f	Frequency
FS	Focal point size indicator	c	Sound velocity
SLI	Sidelobe interference indicator	b	Source bias
L	Array aperture	d	Elements spacing
ρ	Density	d_{AS}	Source-to-array distance

References

1. Hu, Z., Huang, J., Xu, P., Nan, M., Lou, K., et al. (2021). Underwater Acoustic Source Localization via Kernel Extreme Learning Machine. Frontiers in Physics, 9, 653875.
2. Anderson, B.E., Griffa, M., Larmat, C., Ulrich, T.J., Johnson, P.A. (2008). Time Reversal. Acoustics Today, 4(28), 5-16.
3. Li, S., Li, T., Liu, S. (2017). Phase-conjugate arrays and phase-conjugated fields produced by the arrays. Chinese Journal of Ship Research, 12(1), 107-115 (133).
4. Gan, W.S. (2021). Time Reversal Acoustics. Singapore: Springer Nature Singapore.
5. Dowling, D.R., Jackson, D.R. (1998). Phase conjugation in underwater acoustics. The Journal of the Acoustical Society of America, 89(1), 171-181.

6. Rossing, T.D. (2014). Springer Handbook of Acoustics. New York: Springer.
7. Kuperman, W.A., Hodgkiss, W.S., Song, H.C. (1998). Phase conjugation in the ocean: Experimental demonstration of an acoustic time-reversal mirror. The Journal of the Acoustical Society of America, 103(5), 25-40.
8. Fink, M., Cassereau, D., Derode, A., Prada, C., Roux, P., et al. (2000). Time-reversed acoustics. Reports on Progress in Physics, 63, 1933–1995.
9. De Rosny, J., Fink, M. (2007). Focusing properties of near-field time reversal. Physical Review A, 76(6), 637-640.
10. Fannjiang, A.C. (2009). On time reversal mirrors. Inverse Problems, 25(9), 095010.
11. Harker, B.M., Anderson, B.E. (2013). Optimization of the array mirror for time reversal techniques used in a half-space environment. The Journal of the Acoustical Society of America, 133(5), EL351.
12. Yang, T.C. (2002). Temporal resolutions of time-reversal and passive-phase conjugation for underwater acoustic communications. IEEE Journal of Oceanic Engineering, 28(2), 229-245.
13. Godin, O.A., Katsnelson, B.G., Qin, J., Brown, M.G., Zabotin, N.A., et al. (2017). Application of time reversal to passive acoustic remote sensing of the ocean. Acoustical Physics, 63(3), 309-320.
14. Walker, S.C., Kuperman, W.A., Roux, P. (2006). Active waveguide Green's function estimation with application to time-reversal focusing without a probe source in a range-independent waveguide. The Journal of the Acoustical Society of America, 120(5), 2755-2763.
15. Rouseff, D., Jackson, D.R., Fox, W.L.J., Jones, C.D., Ritcey, J.A., et al. (2001). Underwater acoustic communication by passive-phase conjugation: theory and experimental results. IEEE Journal of Oceanic Engineering, 26(4), 821-831.
16. Hodgkiss, W.S., Song, H.C., Kuperman, W.A., Akal, T., Ferla, C., et al. (1999). A long-range and variable focus phase-conjugation experiment in shallow water. The Journal of the Acoustical Society of America, 105(3), 1597-1604.
17. Morse, P.M., and Ingard, K.U. (1968). Theoretical acoustics. Princeton: Princeton University Press.
18. Booth N.O., Abawi A.T., Schey P.W., and Hodgkiss W.S. (2000). Detectability of low-level broad-band signals using adaptive matched-field processing with vertical aperture arrays. IEEE Journal of Oceanic Engineering, 25(3), 296-313.
19. Gemba K.L., Hodgkiss W.S., and Gerstoft P. (2017). Adaptive and compressive matched field processing. The Journal of the Acoustical Society of America, 141(92), 92-103.
20. Hursky P., Hodgkiss W.S., and Kuperman W.A. (2001). Matched field processing with data-derived modes. The Journal of the Acoustical Society of America, 109(4), 1355-1366.